

Article

Numerical Study of Premixed POE₃₋₄/CH₄ Flames at Engine-Relevant Conditions

Yupeng Leng¹, Xiang Ji², Chengcheng Zhang², Nigel Simms¹ , Liming Dai^{2,*} and Chunkan Yu³

¹ School of Water, Energy and Environment, Cranfield University, Cranfield MK43 0AL, UK; yupeng.leng@cranfield.ac.uk (Y.L.); n.j.simms@cranfield.ac.uk (N.S.)

² School of Energy and Power Engineering, Jiangsu University, Zhenjiang 212013, China; jixiang2@tzpec.com.cn (X.J.); zcc_cool@126.com (C.Z.)

³ Institute of Technical Thermodynamics, Karlsruhe Institute of Technology, Engelbert-Arnold-Str. 4, 76131 Karlsruhe, Germany; chunkan.yu@kit.edu

* Correspondence: liming_dai@ujs.edu.cn

Abstract: Polyoxymethylene dimethyl ether (PODE_n, $n \geq 1$) is a promising alternative fuel to diesel with higher reactivity and low soot formation tendency. In this study, POE₃₋₄ is used as a pilot ignition fuel for methane (CH₄) and the combustion characteristics of POE₃₋₄/CH₄ mixtures are investigated numerically using an updated POE₃₋₄ mechanism. The ignition delay time (IDT) and laminar burning velocity (LBV) of POE₃₋₄/CH₄ blends were calculated at high temperature and high pressure relevant to engine conditions. It is discovered that addition of a small amount of POE₃₋₄ has a dramatic promotive effect on IDT and LBV of CH₄, whereas such a promoting effect decays at higher POE₃₋₄ addition. Kinetic analysis was performed to gain more insight into the reaction process of POE₃₋₄/CH₄ mixtures at different conditions. In general, the promoting effect originates from the high reactivity of POE₃₋₄ at low temperatures and it is further confirmed in simulations using a perfectly stirred reactor (PSR) model. The addition of POE₃₋₄ significantly extends the extinction limit of CH₄ from a residence time of ~0.5 ms to that of ~0.08 ms, indicating that the flame stability is enhanced as well by POE₃₋₄ addition. It is also found that NO formation is reduced in lean or rich flames; moreover, NO formation is inhibited by too short a residence time.

Keywords: POE/CH₄ mixture; ignition delay time; laminar burning velocity; kinetic analysis; perfectly stirred reactor



Citation: Leng, Y.; Ji, X.; Zhang, C.; Simms, N.; Dai, L.; Yu, C. Numerical Study of Premixed POE₃₋₄/CH₄ Flames at Engine-Relevant Conditions. *Fuels* **2024**, *5*, 90–106. <https://doi.org/10.3390/fuels5010006>

Academic Editor: Elna Heimdal Nilsson

Received: 22 December 2023

Revised: 5 February 2024

Accepted: 1 March 2024

Published: 12 March 2024



Copyright: © 2024 by the authors. Licensee MDPI, Basel, Switzerland. This article is an open access article distributed under the terms and conditions of the Creative Commons Attribution (CC BY) license (<https://creativecommons.org/licenses/by/4.0/>).

1. Introduction

With the consumption of petroleum resources and the enhancement of environmental awareness, clean utilization of energy in internal combustion engines is becoming a significant issue [1,2]. Therefore, it is urgent to explore renewable alternative fuels such as nature gas [3], ammonia [4], hydrogen [5], methanol [6], and biodiesel [7]. The renewable oxygenated fuel polymethoxydimethyl ethers (PODE_n) are also considered as promising alternative fuels owing to their excellent combustion performance and low soot emissions [8]. Based on life cycle assessment reports, PODE_n derived from biomass can significantly reduce greenhouse gas emissions compared to diesel [9]. PODE_n usually consist of PODE₁₋₆ and the composition varies using different production methods [10]. PODE₃₋₄ are the most desirable components in the mixtures due to their excellent physical and chemical properties [11], which can be used as a fuel additive or burned directly in the engines. Recent studies have demonstrated that diesel/PODE₃₋₄ fuel mixtures can significantly improve the combustion process and reduce unburned hydrocarbon (UHC) and soot emissions because of the oxygen self-supplying effect [12–14], but there is a trade-off relationship between a particular number and nitrogen oxide (NO_x) emissions [15]. At present, PODE_n are primarily used as fuel additives to boost the engine performance considering the limited production of PODE_n [16,17]. Li et al. [18] found that adding 10 vol% POE to diesel

does not cause power reduction in the diesel engine. The researchers [19,20] tested the effects of blending 10–30 vol% PODE₃₋₄ with diesel in a light-duty diesel engine; the results showed that this blending could improve engine efficiency and significantly reduce soot and CO emissions. Ma et al. [21] investigated the spray combustion characteristics of PODE/diesel blends with 0–100 vol% PODE in high-speed OH chemiluminescence and planar laser-induced glow under different ambient conditions. The results showed that, as the PODE content increased, there was also an increase in the flame lift-off length. When the PODE content exceeded 50%, there was almost no soot emission in any of the test cases. Meanwhile, PODE can not only reduce soot formation but also accelerate the oxidation of soot. Lin et al. [22] tested diesel/PODE₃ blends of 0–30 vol% in a CI engine and found that addition of 10 vol% PODE₃ can reduce the particles in emissions. Liu et al. [15] numerically investigated the emission characteristics of PODE/methanol mixtures and found that NO_x emissions increased due to a higher production rate of H and OH radicals formed at higher flame temperatures.

Combustion flames allow the study of flame development, combustion temperatures, and soot formation, all of which can provide the basis for practical engine studies. However, it is not enough to study the combustion flame alone; the combustion mechanism can reveal the fuel consumption, the reaction pathways of the species, the mechanisms of emission formation, and the influence of (-CH₂O-) chain length. In addition, combustion mechanisms can also support the study of IDT and LBV. Current research on the chemical reaction mechanism of PODE focuses on the IDT and the concentration distribution of combustion process components.

Zhang et al. [23] and Hu et al. [24] studied the IDT of PODE₁ at high pressure and argon dilution conditions in a shock tube; Jacobs et al. [25] measured the IDT of PODE₁ under engine-related conditions using a shock tube; in addition, they extended the study conditions of the IDT using a rapid compression machine ($T = 590\text{--}1215\text{ K}$, $p = 10, 20,$ and 40 bar , and $\varphi = 1$); Herzler et al. [26] measured the IDT of an undiluted PODE₁/air mixture at high pressure (30 bar) in a shock tube.

Dagaut et al. [27] studied the oxidation of PODE₁ on a jet stirred reactor at a pressure of 5.07 bar, temperature of 800–1200 K, and equivalence ratios (φ) of 0.444, 0.889, and 1.778, respectively, and obtained the concentration distribution of some intermediate components; Sun and Wang et al. [28] studied the component concentration variation of the combustion process of PODE₃/O₂ at low pressure ($p = 33.3\text{ mbar}$) and 50% argon dilution in a McKenna burner; Sun and Tao et al. [29] studied the reaction pathways and the concentration distribution of intermediate components in PODE₁/O₂/Ar mixtures at low pressure, lean combustion ($p = 750\text{ Torr}$; $\varphi = 0.5$), and high-pressure conditions ($p = 10\text{ atm}$, $\varphi = 0.2, 0.5,$ and 1.5) on a jet stirred reactor; Vermeire et al. [30] studied the oxidation of PODE₁ on a jet stirred reactor at a pressure of 1.07 bar, temperature of 500–1000 K, and φ of 0.25, 1.0, 2.0, and ∞ , respectively; Golka et al. [31] studied the single-molecule pyrolysis of PODE₁ at a pressure of 1 bar and a temperature of 1000–1700 K. The concentration–time profiles of important intermediate components such as CO, CH₂O, and C₂H₆ were recorded; Peukert et al. [32] measured the product distribution during the decomposition of PODE₁ at a pressure of 1.2–2.5 bar and a temperature of 1100–1430 K in a shock tube. Gaiser et al. [33] investigated the effect of different CH₂O polymerization levels on the component concentration distribution during laminar flame of PODE at low pressures in a McKenna burner.

In recent years, basic combustion studies on PODE have mainly focused on unit fuels, and the combustion characteristics of PODE blended with other fuels have not been sufficiently studied; only Herzler et al. [26] reported that the PODE₁/CH₄ mixture was measured in a shock tube at temperatures from 600 to 1500 K, pressures of 30 bar, and φ of 0.5, 1.0, 2.0, and 10. In addition, Zhang et al. [34] recently investigated the intermediate component concentration distribution of PODE₁-blended CH₄ dual fuel during combustion under low pressure and rich combustion conditions on the same burner used by Gaiser et al. [33]. No studies on the combustion characteristics of PODE-

blended CH₄ at a higher temperature and pressure have been reported in the literature, and previous basic combustion studies mainly used argon as the dilution gas, neglecting the NO_x emissions during fuel combustion, whereas, in the engine combustion experiments by Liu et al. [15], it was pointed out that NO_x emissions should be the focus of PODE combustion emission studies. The aim of this paper is, therefore, to extend the data on PODE-blended combustion under different operating conditions and to investigate the mechanism of NO_x emissions from the mixture.

2. Numerical Approach

In this study, the experimental data reported in the literature were used to assess the accuracy of the mechanisms of Cai et al. [35], Jacobs et al. [25], Sun et al. [28], Zhang et al. [34], and He et al. [36]. The mechanism of Cai et al. [35] was finally chosen to study the NO_x emission characteristics of PODE/CH₄/air mixtures because it has the best performance in predicting the measured IDT, LBV, and species profiles from the literature, and it is one of the few chemical reaction mechanisms that include PODE₁₋₄. The numerical simulations in this study were conducted using the open-source package Cantera [37]. The 'Brute Force' method is used to determine the sensitivity coefficient (S_i) for a given reaction as follows.

$$S_i = \frac{k_i}{\Delta_i} \times \frac{\partial \Delta_i}{\partial k_i} \quad (1)$$

where $\partial \Delta_i$ represents the change in a combustion characteristic, such as IDT, LBV, or species component concentration, resulting from a change in the rate constant ∂k_i for the i th reaction. By varying the rate constant k_i for the i th reaction, the change in a particular combustion characteristic resulting from this change is calculated as Δ_i and S_i is the normalized sensitivity coefficient. When the sensitivity coefficient (S_i) is positive, this indicates that the i th reaction promotes ignition, combustion, or the production of a component and, when the sensitivity coefficient is negative, this indicates that the i th reaction inhibits ignition, combustion, or the production of a component.

3. Verification of Chemical Mechanisms

Table 1 shows the physical and chemical properties of PODE₁–PODE₆, which demonstrate the unique advantages of the high oxygen content and high cetane number of PODE_n, a class of excellent fuels. PODE fuels have shown the ability to be used in a diesel engine to reduce soot and emissions. However, when using PODE₁ in the engines, the physical properties, such as boiling point, vapor pressure, and solubility, cause a complex reform of the injection system. The practical use of PODE₂ is limited due to its low flash point. In addition, the flowability of the PODEs decreases as the number of (-CH₂O-) units increases, so the use of longer PODE_n ($n > 5$) carries the risk of fuel system plugging when temperature is low. Therefore, the PODEs fuels used in practice are mainly mixtures of PODE₃ and PODE₄. In this paper, the fraction of the actual PODE_n fuel with $n \geq 5$ is ignored and is considered as a mixture of PODE₃ and PODE₄ [25,38]. In order to investigate the combustion characteristics of PODE₃₋₄ and their blends of CH₄, several PODE₃₋₄ mechanisms are verified against the experimental data of IDT, LBV, and species profiles of flames from the literature.

Figure 1 shows the simulated and experimental results of ignition delay times as a function of pressure at $\varphi = 0.5, 1, \text{ and } 2$ and $p = 10$ and 20 bar, respectively. As illustrated in Figure 1, the ignition delay time decreases with increasing temperature at all four conditions. The mechanism of Sun et al. [29] has a significant overestimation by factors of ~ 10 in predicting the IDT of the PODE₃/air mixture, the mechanism of He et al. [36] also overestimates by nearly 90%, and the mechanism of Niu et al. [39] has a significant increase in calculated values near the equivalence ratio of 1.2 compared to the mechanism of Cai et al. [35]. The mechanism of Niu et al. [39] showed a significant increase in the calculated value when the temperature is around 900 K compared to that of Cai et al. [35], increasing the deviation value from the experimental data. In this paper, the mechanism of

Cai et al. [35] has the best agreement with the experiment data. Sensitivity analysis was used to identify the reactions that have a large influence on the PODE₃/air mixture ignition process, and appropriate modifications to the reaction rates for the first step of the PODE₃ decomposition reaction improved the predictive ability of the mechanism (the updated reactions and parameters are shown in Table 2), especially for the PODE₃/air ignition process at low pressure. The Cai mechanism [35] is modified and the optimized mechanism is represented by Cai* in the next sections. Figure 1 shows that the optimized Cai* mechanism agrees better with the experiment data compared with the Cai mechanism [35]; when comparing the Cai mechanism [35] and the Cai* mechanism to the experiment data, the Cai mechanism [35] has an average deviation of 17.84%, 5.89%, 6.82%, and 37.45% higher than the Cai* mechanism, which illustrates that the Cai* mechanism is more superior at IDT predicting, especially at lean and low pressure condition.

Table 1. Physical properties of PODE₁₋₆ and diesel [39].

Items	Density at 25 °C (kg/m ³)	Cetane Number	Oxygen Content (wt%)	Melting Point °C	Boiling Point °C
PODE ₁	860	29	42.1	−105	42
PODE ₂	960	63	45.3	−65	105
PODE ₃	1020	78	47.1	−41	156
PODE ₄	1060	90	48.2	−7	202
PODE ₅	1100	100	49	18.5	242
PODE ₆	1130	104	49.6	58	280
Diesel	830	46	0	−29	180–370

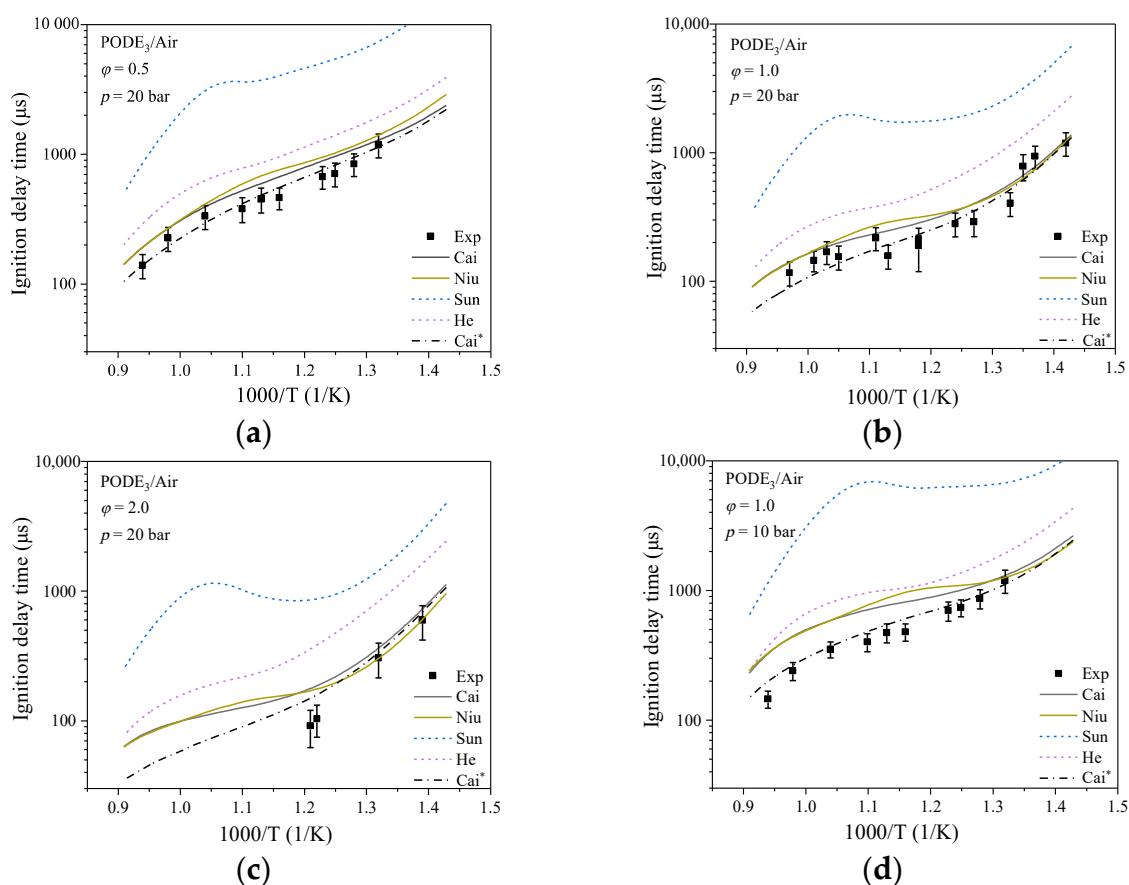


Figure 1. IDT for PODE₃/air: (a) $\phi = 0.5$, $p = 20$ bar; (b) $\phi = 1.0$, $p = 20$ bar; (c) $\phi = 2.0$, $p = 20$ bar; (d) $\phi = 1.0$, $p = 10$ bar. Experimental data are from the shock tube experiments of Cai et al. [35] and mechanisms are from Cai et al. [35], Niu et al. [39], Sun et al. [29], and He et al. [36].

Table 2. Updates in the Cai mechanism [40,41]. Units are s, mol, cm, and cal in $k = AT^n \exp(-\frac{E_a}{RT})$.

No.	Reaction	A	n	Ea
1	$\text{CH}_3 + \text{PODE}_3 = \text{CH}_4 + \text{PODE}_3\text{C}$	2000.00	3.12	7985.66
2	$\text{CH}_3\text{O}_2 + \text{PODE}_3 = \text{CH}_3\text{O}_2\text{H} + \text{PODE}_3\text{B}$	905.00	3.16	11,759.08
3	$\text{PODE}_3 + \text{CH}_3 = \text{PODE}_3\text{A} + \text{CH}_4$	0.60	4.25	7543.74

Figure 2 shows the calculated results for the PODE₄/air mixture from the mechanism of Cai* and Niu et al. [39]. There is no significant difference between the two; the calculated data from the Cai mechanism [35] have 9.67% and 10.14% higher average deviation than Cai* mechanism when compared to the experiment data [35]. Comparing the experimental and simulated data for different operating conditions, increasing the pressure or increasing the equivalence ratio is beneficial to reduce the IDT of PODE fuel.

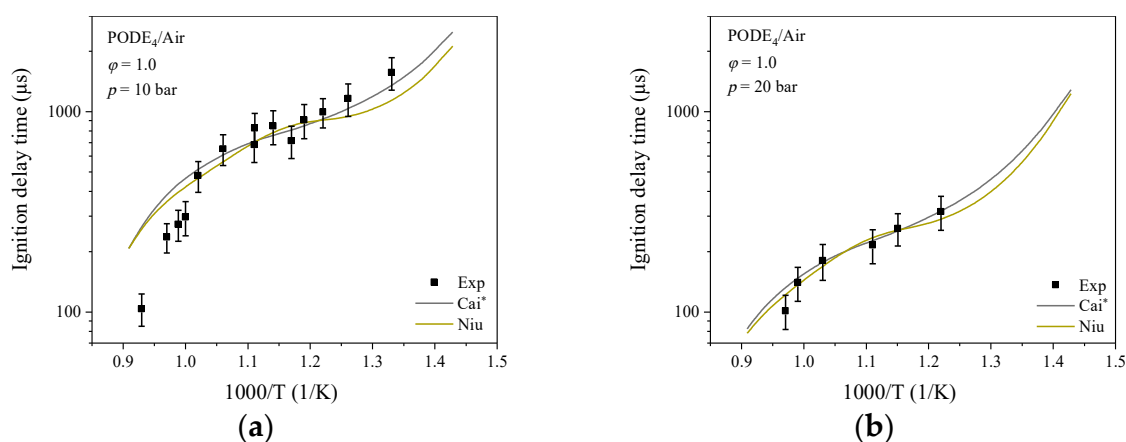
**Figure 2.** IDT for PODE₄/air: (a) $\phi = 1.0, p = 10$ bar; (b) $\phi = 1.0, p = 20$ bar.

Table 3 shows the experimental conditions for the combustion of polymethoxydimethyl ether and its methane-blended mixture in a flame burner reported in the literature [29,35]. In order to gain more insight into the reaction process of PODE₃₋₄/CH₄ mixtures, this study uses the updated Cai* mechanism to calculate the species profile of the mixture combustion process and the laminar burning velocity under different conditions and compares the calculations with experimental data from the literature.

Table 3. Experimental conditions for the combustion of PODE/CH₄ mixtures in a laminar flame (unit: mole fraction).

Mixture	PODE ₁	PODE ₃	CH ₄	O ₂	Ar	Pressure	ϕ	Reference
Mixture 1	0	7.15%	0	42.85%	50%	33.3 mbar	1.0	[29]
Mixture 2	0	11.02%	0	39.01%	49.97%	40 mbar	1.7	[33]
Mixture 3	9.05%	0	9.03%	31.98%	49.94%	40 mbar	1.7	[35]
Mixture 4	3.69%	0	14.76%	31.62%	49.94%	40 mbar	1.4	[35]

Sun et al. [29] and Gaiser et al. [33] studied the component concentration distribution on a Mckenna burner. Figure 3a,b show the component concentration distribution against the height above the burner (HAB), respectively. The Cai* mechanism underestimates the component concentration of the combustion process for CO at an equivalence ratio of 1 and slightly underestimates the component concentration of the combustion endpoint for H₂O and CO₂ at an equivalence ratio of 1.7. The Cai* mechanism is able to accurately predict the species profile of the PODE₃/air flame.

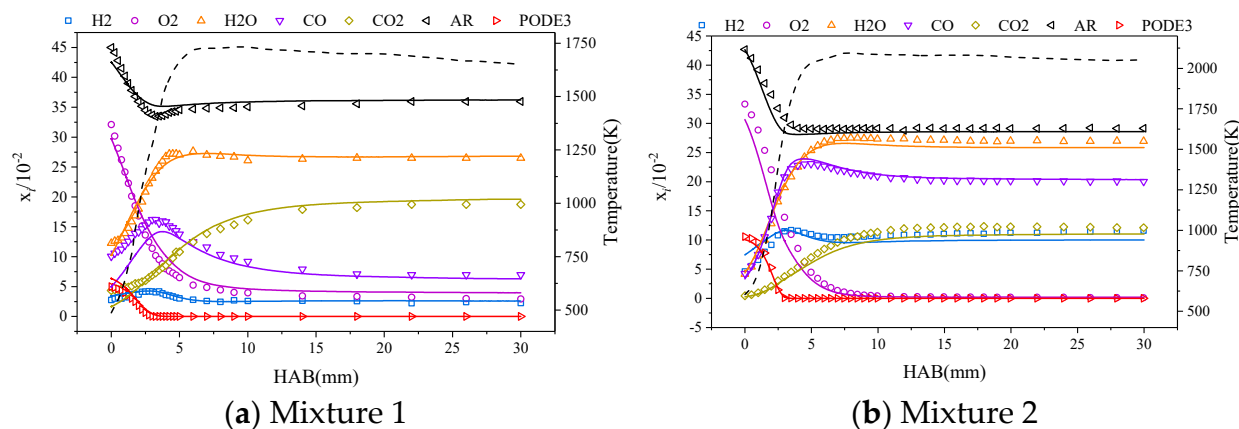


Figure 3. Variation in component concentrations during combustion of mixtures 1 and 2; experimental data for mixtures 1 and 2 from Sun et al. [29] and Gaiser et al. [33] on the Mckenna burner, respectively.

In order to verify the accuracy of the Cai* mechanism in predicting the combustion process of PODE/CH₄ blended fuels, Figure 4 shows the variation in component concentrations during the combustion process of PODE₃₋₄/CH₄ blended fuels. Under the condition of blending PODE with 50% CH₄, the calculated results of the Cai* mechanism are consistent with the experimental data and, when the percentage of CH₄ reaches 80%, the Cai* mechanism for H₂O, CO, and O₂ component concentrations are predicted with deviations of up to approximately 5% molar fraction. Due to the different reactivity of PODE₃₋₄ and methane and the different rates of combustion consumption, at lower temperatures, the CH₄ reaction rate is lower, meaning that, near the flame face, CH₄ barely reacts; as the temperature increases, the CH₄ reaction rate rises and reaches the end of combustion ahead of PODE₃₋₄.

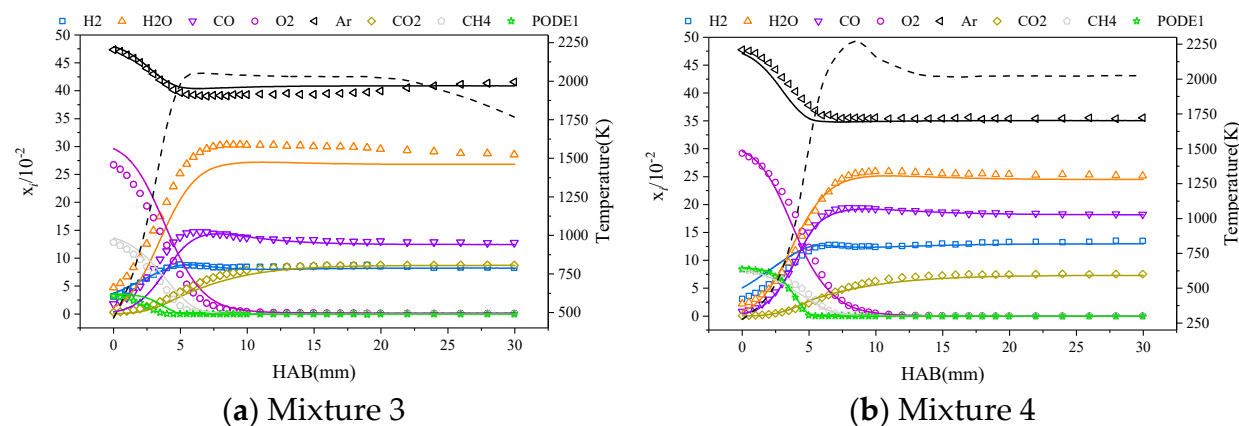


Figure 4. Variation in component concentrations during combustion of mixtures 3 and 4, with experimental data for mixtures 3 and 4 from the Mckenna burner experiments of Zhang et al. [34].

LBV is one of the important indicators of fuel combustion performance. In the absence of data on laminar combustion of PODE₃₋₄/CH₄ mixture, this paper only verifies the calculation results of the Cai* mechanism for PODE₃/air mixture at initial temperature $T = 408$ K and initial pressure $p = 1$ atm; as shown in Figure 5, the calculations of Cai* mechanism agrees well with the experimental data.

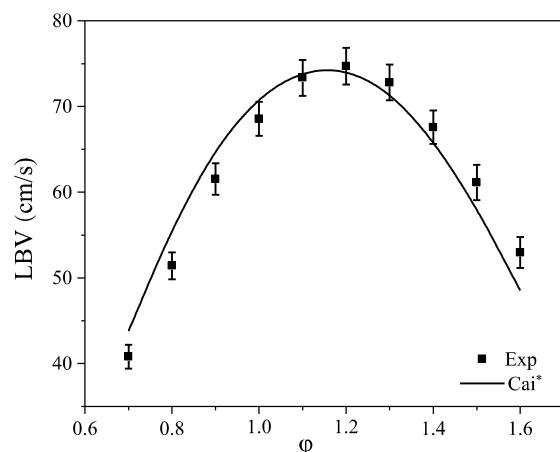


Figure 5. PODE₃/air premixed LBV at 408 K and 1 atm. Experimental data from Cai et al. [35].

4. Results and Discussion

4.1. Combustion Characteristics of PODE₃₋₄/CH₄ at Engine-Relevant Conditions

The effect of the proportions of PODE₃ and PODE₄ in the PODE₃/PODE₄ mixtures on the IDT is shown in Figure 6. As the proportion of PODE₃ and PODE₄ in the fuel changes, the O element in the fuel increases with the proportion of PODE₄ and the fuel chain length has the greatest effect on the IDT of the mixture near the temperature of 1000 K. Under this operating condition, the IDT of pure PODE₃ is about 200 μ s shorter than that of pure PODE₄. When the initial pressure increases to 40 bar, the difference in IDT between the different fuel ratios decreases. Overall, the IDT of the PODE₃₋₄ mixture increases slightly with increasing CH₂O polymerization and, in practice, the effect of the PODE₃ and PODE₄ percentage on the ignition delay level of the fuel can be negligible under the condition that the concentration of PODE₃ and PODE₄ in the PODE₃₋₄-blended fuel is guaranteed.

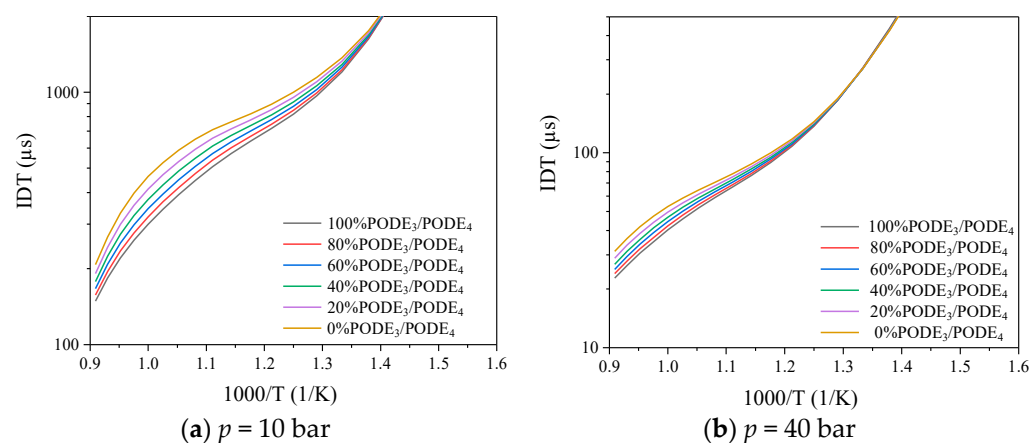


Figure 6. Effect of temperature on IDT of PODE₃/PODE₄ mixtures at ϕ of 1.

PODE₃₋₄ fuels are not suitable for direct use as engine fuels due to their low calorific value (around 45% per mole compared with diesel) and high oxygen content, which tends to cause rough combustion. Theoretically, the high activity of PODE₃₋₄ fuel helps to improve the disadvantages of slow combustion and long IDT of CH₄, and methane itself is a potential carbon-neutral fuel; therefore, in this paper, the Cai* mechanism is used, which has good validation results above, to study the basic combustion characteristics of PODE₃₋₄ and CH₄ blends under general engine operating conditions, and the PODE₃₋₄ fuels mentioned below are blends with a molar fraction share of 80% PODE₃/20% PODE₄.

Figure 7 shows the effect of different initial temperatures on the IDT of the mixture. The addition of 5%PODE₃₋₄ to CH₄ reduces the IDT of the mixture to about 1/10 of its original

value. Continuously increasing the proportion of PODE₃₋₄ in the fuel further reduces the IDT, but the reduction gradually decreases, and, when the proportion of PODE₃₋₄ reaches 60%, the IDT is very close to that of the pure PODE₃₋₄ fuel. The IDT of the mixture gradually decreases with increasing initial temperature and its logarithm is roughly linear with the inverse of the temperature, especially at higher CH₄ percentages. As the initial pressure of the mixture increases from 10 bar to 40 bar, the IDT decreases significantly by approximately one order of magnitude at high pressures compared to low pressures. Due to the low calorific value and high cost of PODE₃₋₄ fuel, a PODE₃₋₄ addition ratio of around 20% is most appropriate when balancing fuel economy and ignition characteristics.

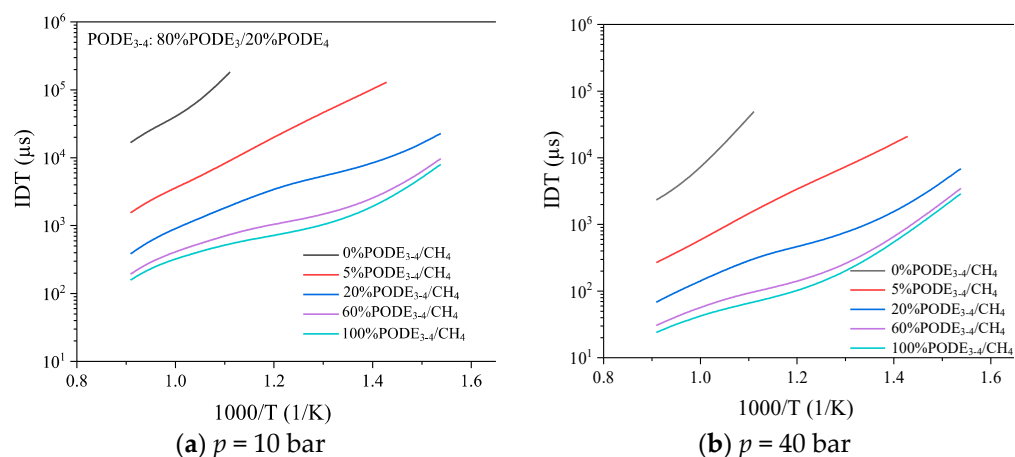


Figure 7. Effect of temperature on the IDT of PODE₃₋₄/CH₄ fuel blends at $\phi = 1$.

To further understand the main reactions controlling the ignition of the PODE₃₋₄/CH₄ fuel mixture, the decomposition reaction of C₂H₆ (C₂H₆ (+M) = 2CH₃ (+M)) has the strongest inhibitory effect on the ignition of the mixture at an initial pressure of 10 bar, followed by the reduction reaction of methyl to methane, as shown in Figure 8a. The reaction H₂O₂ (+M) = 2OH (+M) is the strongest promoter of mixture ignition, followed by the reaction CH₃ + CH₃O₂ = 2CH₃O. Several of the above dominant mixture ignition reactions show varying degrees of decrease in sensitivity coefficients as the pressure increases. The reaction 2HO₂ = H₂O₂ + O₂ replaces the reaction C₂H₆ (+M) = 2CH₃ (+M) as the strongest ignition inhibiting reaction when the initial pressure is increased to 40 bar. Three different dehydrogenation reactions of the PODE₃₋₄ fuel molecule show broadly similar ignition-promoting abilities, with the sensitivity of these three reactions increasing slightly as the initial pressure is increased. Overall, the reactions that control the ignition of the mixture are mainly oxidation or reduction reactions containing C components, with the fuel dehydrogenation-derived macromolecular reactions playing an important role in the ignition of the fuel mixture. As shown in Figure 8b, the most sensitive reaction of 5%PODE₃₋₄-fuel-added specific mixture during ignition is the same as that of 20%PODE₃₋₄-fuel-added specific mixture, and the sensitivity coefficient of each reaction changes monotonically with the addition ratio of PODE₃₋₄ fuel.

In order to understand the effect of different initial pressures and PODE₃₋₄ fuel shares on the IDT of the mixture, a curve of the PODE₃₋₄/CH₄ mixture with the ϕ at an initial temperature of 408 K is shown in Figure 9. The IDT differs from the LBV in that the former is mainly influenced by the reaction of cracking of fuel molecules or the reaction of further oxidation of macromolecular derivatives produced by fuel. As PODE₃₋₄ is a highly oxygenated fuel, its own pyrolysis and elemental recombination can generate a large number of highly reactive radicals, which further promote its own ignition and accelerate the oxidation of CH₄ fuel; thus, the addition of a small amount of PODE₃₋₄ can significantly reduce the IDT of the mixture. The LBV, as shown in Figure 9, is mainly controlled by the small-molecule reactive radical in the combustion process, so the addition of a small amount of PODE₃₋₄ does not significantly increase the LBV of the mixture, which varies

roughly linearly with the PODE_{3-4} addition ratio. Since PODE_{3-4} is an oxygenated fuel, as the proportion of PODE_{3-4} in the mixture increases, the peak LBV moves towards a higher equivalence ratio. When the proportion of PODE_{3-4} in the mixture is 20%, the peak LBV of the mixture at an initial pressure of 10 atm is almost half of that at atmospheric pressure; so, in practice, when this fuel mixture is used as engine fuel, the cylinder pressure should not be too high.

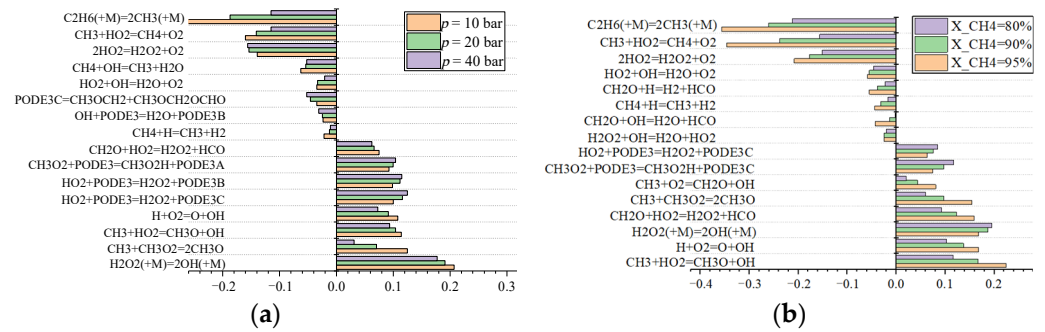


Figure 8. Sensitivity of reactions with a large effect on the IDT of $\text{PODE}_{3-4}/\text{CH}_4$ fuel at an initial temperature of 1000 K.

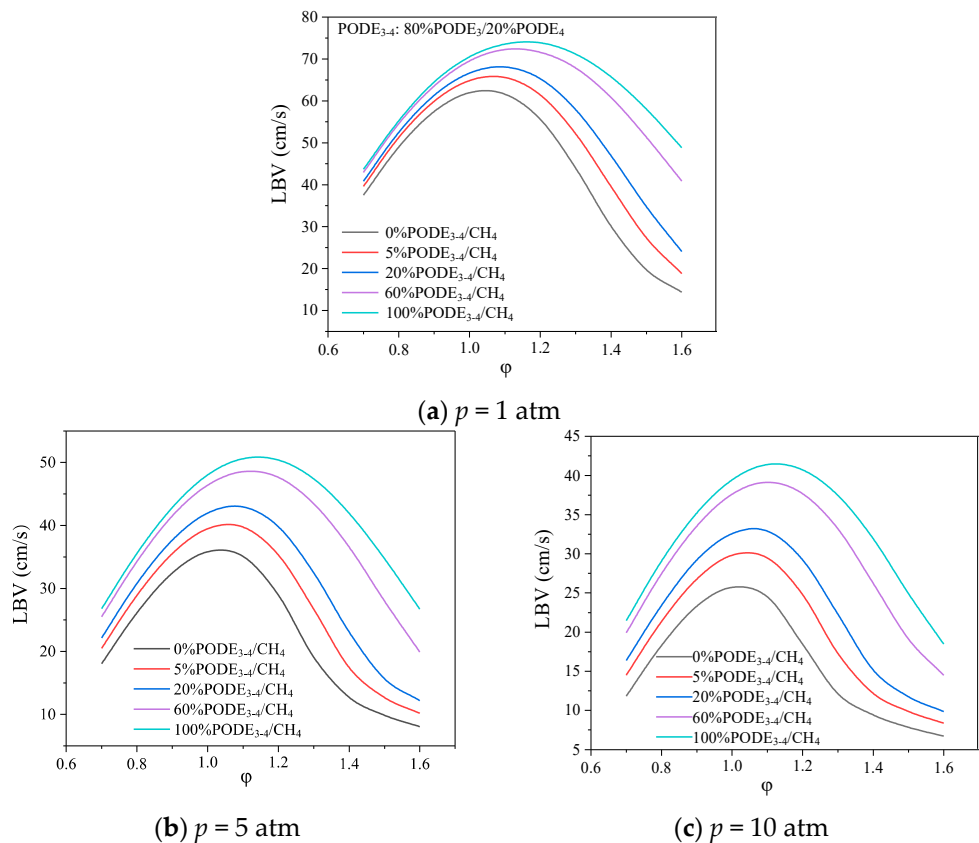


Figure 9. LBV of $\text{PODE}_{3-4}/\text{CH}_4$ mixture at an initial temperature of 408 K.

To further understand the main reactions controlling the LBV of the $\text{PODE}_{3-4}/\text{CH}_4$ mixture, the reaction $\text{H} + \text{O}_2 = \text{O} + \text{OH}$ is the strongest contributor to the combustion of the mixture and is almost two to three times more sensitive than the second strongest contributor, $\text{CO} + \text{OH} = \text{CO}_2 + \text{H}$, as shown in Figure 10a. At atmospheric pressure, the reaction $\text{H} + \text{HCO} = \text{CO} + \text{H}_2$ has the strongest inhibitory effect on the combustion of the gas mixture, which increases with increasing pressure, and, at high-pressure 10 atm working conditions, the reaction $\text{CH}_3 + \text{H} (+\text{M}) = \text{CH}_4 (+\text{M})$ replaces this reaction in

showing the strongest inhibitory effect. As the pressure increases, the sensitivity of the reactions $\text{CH}_3 + \text{H} (+\text{M}) = \text{CH}_4 (+\text{M})$ and $\text{H} + \text{O}_2 (+\text{M}) = \text{HO}_2 (+\text{M})$ both show a larger increase, which means that their inhibition to the combustion of the mixture increases, which is one of the possible factors leading to the decrease in the flame speed with the increase in the initial pressure. As shown in Figure 10b, variations in the PODE_{3-4} fuel addition ratio, when not exceeding 20%, have little effect on the sensitivity of reactions that have a large impact on the LBV of the mixture.

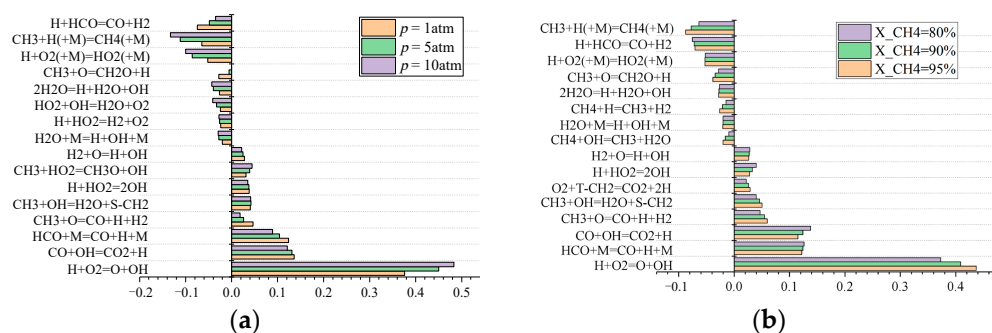


Figure 10. Sensitivity of reactions with a large effect on the LBV of $\text{PODE}_{3-4}/\text{CH}_4$ at an initial temperature of 408 K: (a) sensitivity analysis with different pressure; (b) sensitivity analysis with different mole fraction of CH_4 .

4.2. Flux Analysis

The reaction pathway for the combustion of $\text{PODE}_3/\text{CH}_4$ mixtures is investigated, according to previous calculation in Figure 6a,b; the $\text{PODE}_3/\text{PODE}_4$ mixture has similar reaction paths to 100% PODE_3 ; therefore, in order to simplify the research, the reaction path of 100% PODE_3 is studied. As shown in Figure 11, PODE_3 is first oxidized by O atoms, H atoms, or OH radical in a dehydrogenation reaction to produce PODE_3A , PODE_3B , and PODE_3C depending on the position of the extracted hydrogen atoms. The flux size shows that the hydrocarbon bond of methyl is more easily broken than that of methoxy, which, in turn, is more easily dehydrogenated than the methoxy located on the outer side of the long chain, and the initial stage reaction path is consistent with the single-fuel reaction path of PODE_3 reported in the literature [28]. The generated PODE_3A undergoes a series of β -cracking to eventually produce CH_2O , and the methyl radical (CH_3) that accompanies this process is slowly consumed at lower temperatures (1200 K) and builds up in large quantities, with a small proportion being reduced to CH_4 . This explains why the CH_4 concentration distribution decreases slowly at the initial stage of the flame, with the large amount of CH_4 oxidized to methyl radical involved in further reactions occurring when the flame temperature reaches 1500 K or higher.

The fuel radical PODE_3B first loses methyl radical ($-\text{CH}_3$) to form a carbon–oxygen double bond, which is one of the few major pathways for the formation of methyl radical during the combustion of PODE_3 fuel, apart from the cleavage of the radical CH_3OCH_2 to form $-\text{CH}_3$. The formation of carbon fume is usually achieved by the gradual dehydrogenation of ethylene from the collision of methyl radical and the gradual formation of acetylene as a precursor to carbon fume via the $\text{CH}_3 \rightarrow \text{C}_2\text{H}_6 \rightarrow \text{C}_2\text{H}_5 \rightarrow \text{C}_2\text{H}_4 \rightarrow \text{C}_2\text{H}_3 \rightarrow \text{C}_2\text{H}_2$ reaction path, while methyl- CH_3 is rarely produced in a low-temperature PODE_3 flame and $-\text{CH}_3$ produced in a high-temperature CH_4 flame is rapidly oxidized and cannot form a precursor to carbon fume. PODE_3C , like PODE_3B , first breaks the carbon–oxygen bond to form an aldehyde radical, which is then dehydrogenated from the aldehyde radical or another carbon chain to produce formaldehyde (CH_2O).

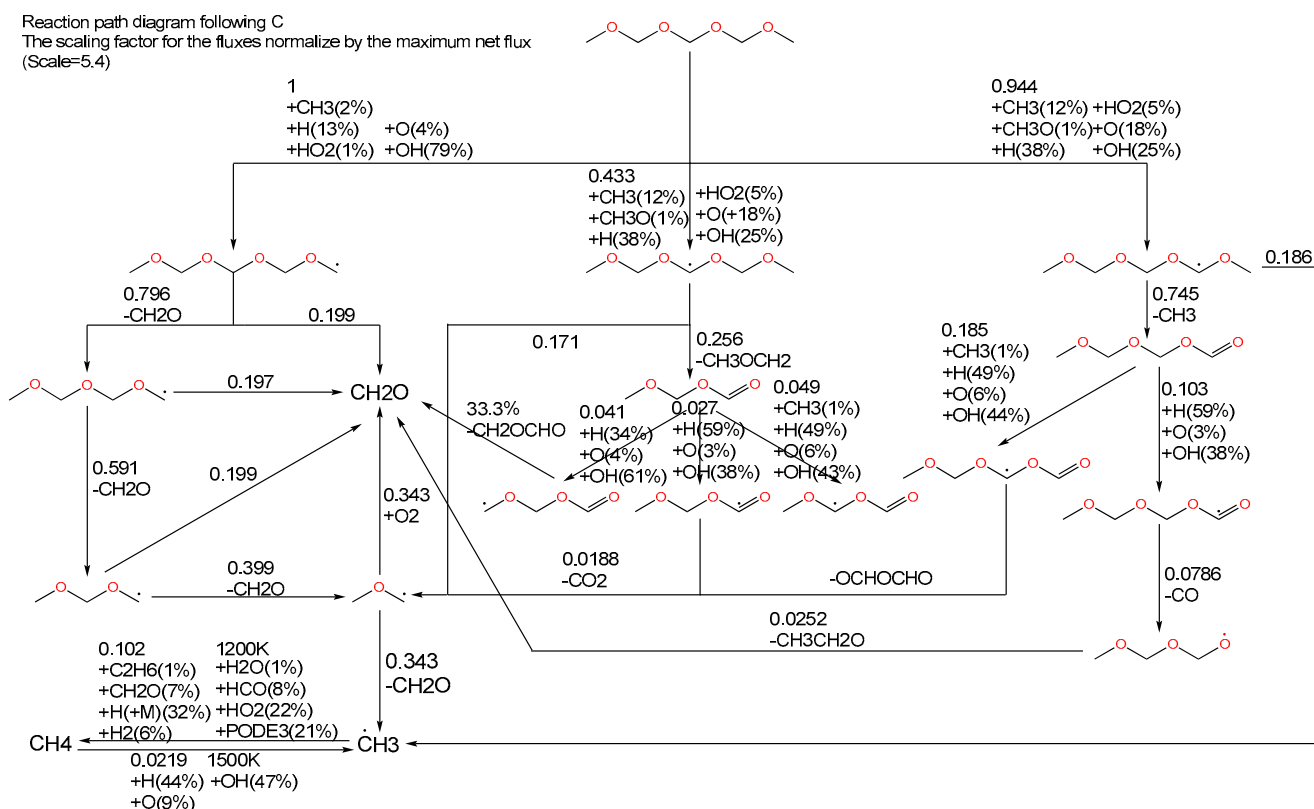


Figure 11. Reaction paths of the PODE₃/CH₄ mixture during laminar flame, taken at the maximum flame temperature gradient. The maximum path flux is defined as 1 and the percentage is the proportion of the reaction in this path. The overall path flux scaling factor is 5.4.

4.3. Analysis of NO_x Emissions from the Combustion of PODE₃/CH₄/Air Mixture

To investigate the effect of fuel fraction and equivalence ratio on NO_x emissions from a PODE₃/CH₄/air mixture, Glarborg's C–N interaction sub-mechanism [42] was added to the mechanism of Cai* in this paper. As shown in Figure 12, the peak NO_x emissions from the combustion of the mixture in air at atmospheric pressure are in the range of approximately 150–180 ppm, and the peak position is not influenced by the oxygen content of the mixture and always occurs near an equivalence ratio of 1. The higher the PODE₃ content in the mixture, the higher the adiabatic flame temperature and the consequent increase in peak NO_x emissions. The NO_x emission shows strong correlation with temperature. As can be seen, the NO_x emissions of the mixture can be reduced significantly at lean or rich conditions.

The elemental N reaction path for a 50% CH₄/50% PODE₃/air mixture with an equivalence ratio of 1 is shown in Figure 13. At the highest flame surface temperature (2300 K shown in Figure 12), NO_x emissions are mainly NO. From the reaction path, at high temperatures, N₂ is directly oxidized by oxygen or OH-reactive radicals to produce NO, a small amount is oxidized to produce N₂O, and a much smaller amount of N₂ is oxidized by H. Analyzing the reaction path, it can be seen that, at this temperature, mainly thermal NO (T-NO) is generated and this is also the peak of NO_x emission from the mixture.

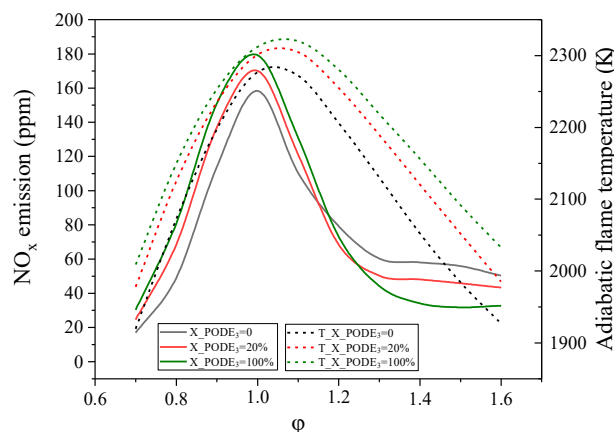


Figure 12. NO_x emissions from a premixed laminar flame of PODE₃/CH₄/air mixture at atmospheric pressure. The solid line is NO_x emissions and the dashed line is the adiabatic flame temperature.

Reaction path diagram following N
 The scaling factor for the fluxes normalize by the maximum net flux
 (Scale=2.5e-05)

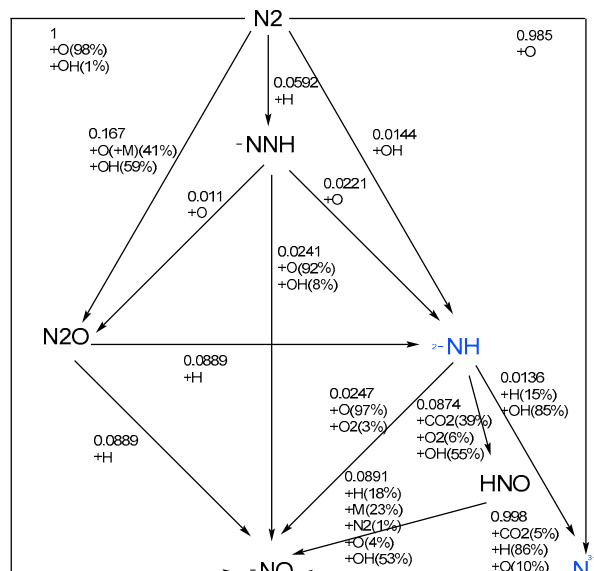


Figure 13. Elemental N reaction path for a premixed laminar flame with a PODE₃/CH₄/air mixture with $\phi = 1$ at atmospheric pressure (Taken at the highest flame temperature).

In a premixed laminar flame PODE₃/CH₄/air mixture with $\phi = 1.5$ at a lower temperature (2000 K as shown in Figure 12), the cyanide generated by the interaction of C and N contributes most of the NO_x production, with the reaction path starting with the CN radical being gradually oxidized to produce NO, mainly fast NO (P-NO), at this temperature in Figure 14. When the gas mixture equivalent ratio is continuously increased, the maximum adiabatic flame temperature decreases and the NO_x emission decreases to a certain level and then remains stable and, as the proportion of CH₄ in the gas mixture increases, the emission gradually increases, which is due to the fact that, at this time, the gas mixture mainly generates CN radicals through the C–N interaction reaction and is then oxidized to produce NO (P-NO) and the flame temperature has less influence on it, while the higher the CH₄ content in the mixture, the higher the content of the generated methyl (CH₃) radicals and the easier it is to react with N elements to form CN.

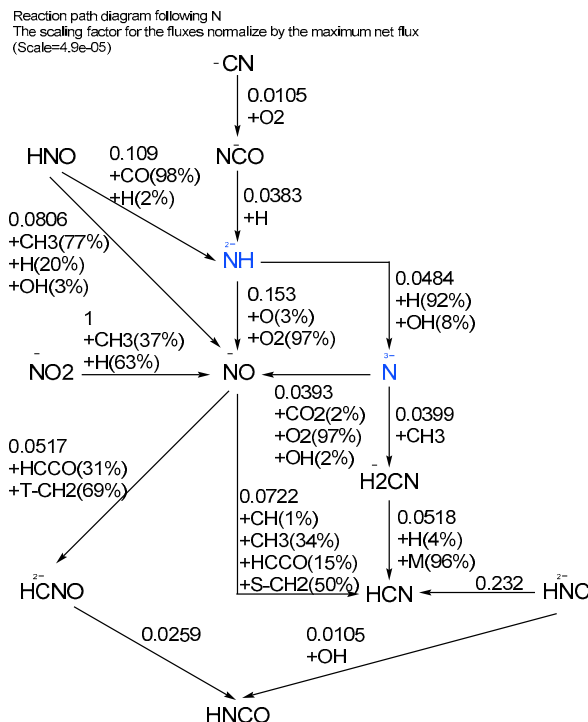


Figure 14. Elemental N reaction path for a premixed laminar flame with a PODE₃/CH₄/air mixture with $\phi = 1.5$ at atmospheric pressure (Taken at the highest flame temperature).

4.4. PSR Simulation of PODE₃₋₄/CH₄ Mixture

In order to predict the extinction of the PODE₃₋₄/CH₄ mixture flame, a perfectly stirred reactor (PSR) model [43] is introduced in this research. The PSR model structures the turbulent intensity of inner gas as flow speed and regulates it by the residence time. The ideal gas reactor module was constructed by the verified chemical reaction kinetics codes from Yu et al. [44] in MATLAB[®]; non-steady-state numerical methods were applied in the simulations and the reactor temperature, pressure, and equivalence ratio of the model are 300 K, 1 atm, and 1, respectively. The composition of the fuel mixtures is shown in Table 4.

Table 4. Properties of PODE₃₋₄/CH₄ mixtures.

No.	Composition of Fuels	LHV of Fuel Mixtures (KJ/mole)	ϕ
1	100% CH ₄ /Air	-726.90	1
2	(80% CH ₄ + 20% PODE ₃)/Air	-738.23	1
3	(80% CH ₄ + 10% PODE ₃ + 10% PODE ₄)/Air	-738.19	1
4	(80% CH ₄ + 20% PODE ₄)/Air	-738.11	1

Figure 15a displays the temperature profiles as a function of the residence time. The ambient temperature in the PSR model is the adiabatic temperature of the studied mixture. The graph illustrates that the temperature of the mixtures gradually decreases when the residence time gets close to the extinction limits. As the ratios of PODE₃ and PODE₄ in the fuel change, the difference between the three blended fuels is insignificant. The addition of PODE₃₋₄ to CH₄ expanded the extinction limit. The temperature curve of pure CH₄ is very close because of the approximate lower heat value.

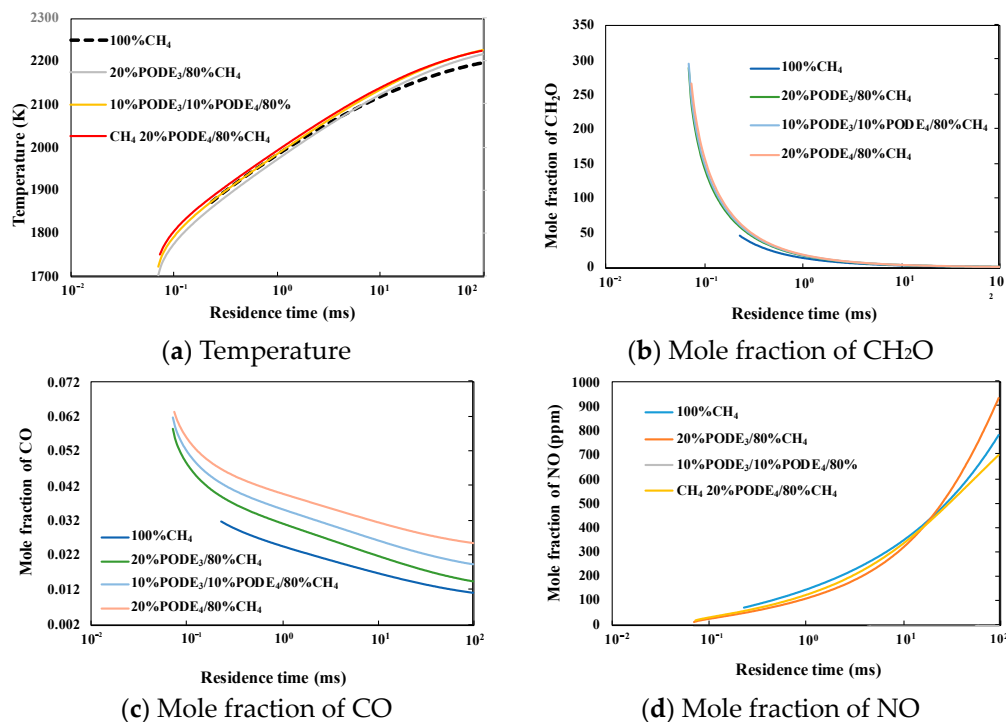


Figure 15. Temperature and mole fraction of key species as a function of the residence time.

Figure 15b–d illustrate the impact of residence time on the mole fraction of CH₂O, CO, and NO. The introduction of PODE₃₋₄ significantly reduces the extinction residence time, but the effect of the variation in PODE₃ and PODE₄ are marginal. When the residence time is approximate to the extinction limit, a rapid increase in the mole fraction of CH₂O is observed; generally, CH₂O appears in the early stage of the combustion of PODE₃₋₄, indicating that the high reactivity of PODE₃₋₄ at low temperature significantly promotes the combustion of methane at a short residence time. Figure 16 also shows that the CO increases when the residence time approaches the extinction limit; it is reasonable because the conversion of CO to CO₂ is hindered by the low flame temperature and short reaction time induced by the short residence time. Figure 16 illustrates the influence of residence on NO generation; there are no N elements in PODE₃₋₄/CH₄ fuels; the thermal NO is caused by the high flame temperature, the temperature decreases when the residence time trends to the extinction limit and, consequently, NO formation is inhibited.

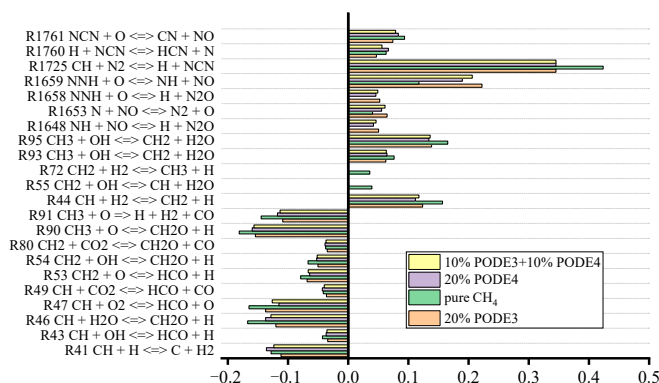


Figure 16. Sensitivity analysis of NO for PODE₃₋₄/CH₄ fuel mixture at atmospheric pressure for equivalence ratios of 1.

This study aims to elucidate how NO is generated under extremely short residence time. Sensitivity analyses of the NO formation using the PSR model are conducted as shown in Figure 16.

As can be seen from Figure 16, when the equivalence ratio equals 1, the C–N interaction reaction $\text{CH} + \text{N}_2 = \text{H} + \text{NCN}$ makes the largest contribution to NO production due to the low flame temperature, followed by $\text{NNH} + \text{O} = \text{NH} + \text{NO}$. The reaction that inhibits NO production the most is $\text{CH}_3 + \text{O} = \text{CH}_2\text{O} + \text{H}$. The reactions that have a large effect on NO are mainly between the elements N and O. The carbon-containing reactions have a smaller effect on NO; most of them are reflected in the competition for H atoms. The influence of C–N interaction reactions on NO production and consumption dominated, in line with the pattern reflected in Figures 14 and 15. In fact, since the $\text{PODE}_{3-4}/\text{CH}_4$ mixture does not contain N elements, there is no fuel-based NO in the combustion process. As pointed out above, NO emissions from the mixture are mainly fast NO (P-NO) at low temperatures and thermal NO (T-NO) at high temperatures, while P-NO is inevitable when air is used as the oxidant.

5. Conclusions

In this study, PODE_{3-4} is used as a pilot ignition fuel for methane (CH_4); the combustion characteristics of $\text{PODE}_{3-4}/\text{CH}_4$ mixtures are investigated numerically at engine-relevant conditions using an optimized PODE mechanism in this study based on the mechanism from Cai et al. [35] and Garblorg mechanism [42]. PODE fuels show great potential in enhancing the combustion properties of CH_4 . The key findings are summarized as follows:

- (1) The calculated IDT of pure PODE_3 and pure PODE_4 are negligible at low flame temperature, whereas at higher temperature ($T > 1000$ K), the calculated IDT of pure PODE_4 are ~10 times longer than that of pure PODE_3 . The difference in the IDTs of PODE_3 and PODE_4 declines at higher pressure ($p = 40$ bar).
- (2) Using a blend consisting of 80% PODE_3 and 20% PODE_4 as pilot ignition fuel, the IDT of CH_4 is significantly reduced and the LBV of CH_4 is substantially increased with increased pilot fuel addition. However, such a promoting effect decays at a higher fraction of PODE_{3-4} addition.
- (3) The NO_x emission is increased with PODE_3 addition; the maximum NO_x emission of pure PODE_3 is ~40 ppm higher than that of pure CH_4 . The NO_x emission is dramatically reduced at lean or rich flames. The PSR simulation shows that the NO_x formation is inhibited at too short a residence time because the flame temperature is too low at that condition, which hinders the thermal NO_x formation.
- (4) The extinction residence time of CH_4 is greatly expanded from 0.5 ms to 0.08 ms by the addition of 20% PODE_{3-4} ; consequently, the high reactivity of PODE fuels at low temperature is vital to enhance the flame stability of CH_4 .

Author Contributions: Conceptualization, L.D. and C.Y.; methodology, Y.L. and L.D.; software, Y.L. and X.J.; validation, X.J. and C.Z.; formal analysis, C.Z.; investigation, Y.L.; data curation, Y.L.; writing—original draft preparation, Y.L.; writing—review and editing, N.S. and L.D.; supervision, N.S.; funding acquisition, L.D. All authors have read and agreed to the published version of the manuscript.

Funding: This research was funded by the National Natural Science Foundation of China (Grant No. 52206149).

Data Availability Statement: The data that support the findings of this study are available from the corresponding author upon reasonable request.

Conflicts of Interest: The authors declare no conflicts of interest.

References

1. Ishida, M.; Yamamoto, S.; Ueki, H.; Sakaguchi, D. Remarkable improvement of NO_x –PM trade-off in a diesel engine by means of bioethanol and EGR. *Energy* **2010**, *35*, 4572–4581. [[CrossRef](#)]
2. Zheng, Z.; Xia, M.; Liu, H.; Shang, R.; Ma, G.; Yao, M. Experimental study on combustion and emissions of n-butanol/biodiesel under both blended fuel mode and dual fuel RCCI mode. *Fuel* **2018**, *226*, 240–251. [[CrossRef](#)]

3. Sattarzadeh, M.; Ebrahimi, M.; Jazayeri, S.A. A detail study of a RCCI engine performance fueled with diesel fuel and natural gas blended with syngas with different compositions. *Int. J. Hydrogen Energy* **2022**, *47*, 16283–16296. [[CrossRef](#)]
4. Dai, L.; Gersen, S.; Glarborg, P.; Levinsky, H.; Mokhov, A. Experimental and numerical analysis of the autoignition behavior of NH₃ and NH₃/H₂ mixtures at high pressure. *Combust. Flame* **2020**, *215*, 134–144. [[CrossRef](#)]
5. Zareei, J.; Rohani, A. Optimization and study of performance parameters in an engine fueled with hydrogen. *Int. J. Hydrogen Energy* **2020**, *45*, 322–336. [[CrossRef](#)]
6. Gao, Z.; Wu, S.; Luo, J.; Zhang, B.; Zhang, H.; Xiao, R. Optimize the co-solvent for methanol in diesel with group of oxygen-containing reagents: Molecular structure and intermolecular forces analysis. *Fuel Process. Technol.* **2021**, *222*, 106980. [[CrossRef](#)]
7. Wu, G.; Wang, X.; Abubakar, S.; Li, Y. A skeletal mechanism for biodiesel-dimethyl ether combustion in engines. *Fuel* **2022**, *325*, 124834. [[CrossRef](#)]
8. Zheng, Y.; Tang, Q.; Wang, T.; Wang, J. Kinetics of synthesis of polyoxymethylene dimethyl ethers from paraformaldehyde and dimethoxymethane catalyzed by ion-exchange resin. *Chem. Eng. Sci.* **2015**, *134*, 758–766. [[CrossRef](#)]
9. Mahbub, N.; Oyedun, A.O.; Kumar, A.; Oestreich, D.; Arnold, U.; Sauer, J. A life cycle assessment of oxymethylene ether synthesis from biomass-derived syngas as a diesel additive. *J. Clean. Prod.* **2017**, *165*, 1249–1262. [[CrossRef](#)]
10. Liu, F.; Wang, T.; Zheng, Y.; Wang, J. Synergistic effect of Brønsted and Lewis acid sites for the synthesis of polyoxymethylene dimethyl ethers over highly efficient SO₄²⁻/TiO₂ catalysts. *J. Catal.* **2017**, *355*, 17–25. [[CrossRef](#)]
11. Bi, X.; Liu, H.; Huo, M.; Shen, C.; Qiao, X.; Lee, C.F. Experimental and numerical study on soot formation and oxidation by using diesel fuel in constant volume chamber with various ambient oxygen concentrations. *Energy Convers. Manag.* **2014**, *84*, 152–163. [[CrossRef](#)]
12. Liu, H.; Wang, Z.; Zhang, J.; Wang, J.; Shuai, S. Study on combustion and emission characteristics of Polyoxymethylene Dimethyl Ethers/diesel blends in light-duty and heavy-duty diesel engines. *Appl. Energy* **2017**, *185*, 1393–1402. [[CrossRef](#)]
13. Li, Y.; Chen, Y.; Wu, G. A new skeletal mechanism for diesel-n-butanol blends combustion in engine. *Fuel* **2020**, *264*, 116856. [[CrossRef](#)]
14. Liu, J.; Yang, J.; Sun, P.; Gao, W.; Yang, C.; Fang, J. Compound combustion and pollutant emissions characteristics of a common-rail engine with ethanol homogeneous charge and polyoxymethylene dimethyl ethers injection. *Appl. Energy* **2019**, *239*, 1154–1162. [[CrossRef](#)]
15. Liu, J.; Ma, H.; Sun, P.; Wang, P.; Wang, T.; Liu, Y.; Wei, M.; Fang, J. Simulation study on in-cylinder combustion and pollutant generation characteristics of PODE/methanol blends. *Fuel Process. Technol.* **2022**, *228*, 107165. [[CrossRef](#)]
16. Hao, Y.; Xinghu, L.I.; Mingfei, M.U.; Xuehao, L.I. Experiments on the performances and emissions of diesel engine fuelled with diesel/polyoxymethylene dimethyl ethers blends. *J. Automot. Saf. Energy* **2015**, *13*, 1053.
17. He, J.; Su, X.; Chen, H.; Chen, Y.; Zhang, X.; Liu, Y.; Tian, Z.; Xu, H. Spray and combustion characteristics of polyoxymethylene dimethyl ethers and diesel blends in a constant volume chamber. *Energy Rep.* **2022**, *8*, 1056–1066. [[CrossRef](#)]
18. Li, X.; Yu, H.; Sun, Y.; Wang, H.; Guo, T.; Sui, Y.; Miao, J.; Zeng, X.; Li, S. Synthesis and Application of Polyoxymethylene Dimethyl Ethers. *Appl. Mech. Mater.* **2013**, *448–453*, 2969–2973. [[CrossRef](#)]
19. Liu, H.; Wang, Z.; Wang, J.; He, X.; Zheng, Y.; Tang, Q.; Wang, J. Performance, combustion and emission characteristics of a diesel engine fueled with polyoxymethylene dimethyl ethers (PODE3-4)/ diesel blends. *Energy* **2015**, *88*, 793–800. [[CrossRef](#)]
20. Liu, J.; Sun, P.; Huang, H.; Meng, J.; Yao, X. Experimental investigation on performance, combustion and emission characteristics of a common-rail diesel engine fueled with polyoxymethylene dimethyl ethers-diesel blends. *Appl. Energy* **2017**, *202*, 527–536. [[CrossRef](#)]
21. Ma, Y.; Cui, L.; Ma, X.; Wang, J. Optical study on spray combustion characteristics of PODE/diesel blends in different ambient conditions. *Fuel* **2020**, *272*, 117691. [[CrossRef](#)]
22. Lin, Q.; Tay, K.L.; Yu, W.; Yang, W.; Wang, Z. Effects of polyoxymethylene dimethyl ether 3 (PODE3) addition and injection pressure on combustion performance and particle size distributions in a diesel engine. *Fuel* **2021**, *283*, 119347. [[CrossRef](#)]
23. Zhang, C.; Li, P.; Li, Y.; He, J.; Li, X. Shock-tube study of dimethoxymethane ignition at high temperatures. *Energy Fuels* **2014**, *28*, 4603–4610. [[CrossRef](#)]
24. Hu, E.; Gao, Z.; Liu, Y.; Yin, G.; Huang, Z. Experimental and modeling study on ignition delay times of dimethoxy methane/n-heptane blends. *Fuel* **2017**, *189*, 350–357. [[CrossRef](#)]
25. Jacobs, S.; Döntgen, M.; Alqaity, A.B.S.; Kopp, W.A.; Kröger, L.C.; Burke, U.; Pitsch, H.; Leonhard, K.; Curran, H.J.; Heufer, K.A. Detailed kinetic modeling of dimethoxymethane. Part II: Experimental and theoretical study of the kinetics and reaction mechanism. *Combust. Flame* **2019**, *205*, 522–533. [[CrossRef](#)]
26. Herzler, J.; Fikri, M.; Schulz, C. High-pressure shock-tube study of the ignition and product formation of fuel-rich dimethoxymethane (DMM)/air and CH₄/DMM/air mixtures. *Combust. Flame* **2020**, *216*, 293–299. [[CrossRef](#)]
27. Dagaut, P.; Cathonnet, M. Oxidation of dimethoxymethane in a jet-stirred reactor. *Combust. Flame* **2001**, *125*, 1106–1117. [[CrossRef](#)]
28. Sun, W.; Wang, G.; Li, S.; Zhang, R.; Yang, B.; Yang, J.; Li, Y.; Westbrook, C.K.; Law, C.K. Speciation and the laminar burning velocities of poly(oxymethylene) dimethyl ether 3 (POMDME3) flames: An experimental and modeling study. *Proc. Combust. Inst.* **2017**, *36*, 1269–1278. [[CrossRef](#)]
29. Sun, W.; Tao, T.; Lailliau, M.; Hansen, N.; Yang, B.; Dagaut, P. Exploration of the oxidation chemistry of dimethoxymethane: Jet-stirred reactor experiments and kinetic modeling. *Combust. Flame* **2018**, *193*, 491–501. [[CrossRef](#)]

30. Vermeire, F.H.; Carstensen, H.H.; Herbinet, O.; Battin-Leclerc, F.; Marin, G.B.; Van Geem, K.M. Experimental and modeling study of the pyrolysis and combustion of dimethoxymethane. *Combust. Flame* **2018**, *190*, 270–283. [[CrossRef](#)]
31. Golka, L.; Weber, I.; Olzmann, M. Pyrolysis of dimethoxymethane and the reaction of dimethoxymethane with H atoms: A shock-tube/ARAS/TOF-MS and modeling study. *Proc. Combust. Inst.* **2019**, *37*, 179–187. [[CrossRef](#)]
32. Peukert, S.; Sela, P.; Nativel, D.; Herzler, J.; Fikri, M.; Schulz, C. Direct Measurement of High-Temperature Rate Constants of the Thermal Decomposition of Dimethoxymethane, a Shock Tube and Modeling Study. *J. Phys. Chem. A* **2018**, *122*, 7559–7571. [[CrossRef](#)]
33. Gaiser, N.; Zhang, H.; Bierkandt, T.; Schmitt, S.; Zinsmeister, J.; Kathrotia, T.; Hemberger, P.; Shaqiri, S.; Kasper, T.; Aigner, M.; et al. Investigation of the combustion chemistry in laminar, low-pressure oxymethylene ether flames (OME0–4). *Combust. Flame* **2022**, *243*, 112060. [[CrossRef](#)]
34. Zhang, H.; Kaczmarek, D.; Rudolph, C.; Schmitt, S.; Gaiser, N.; Oßwald, P.; Bierkandt, T.; Kasper, T.; Atakan, B.; Kohse-Höinghaus, K. Dimethyl ether (DME) and dimethoxymethane (DMM) as reaction enhancers for methane: Combining flame experiments with model-assisted exploration of a polygeneration process. *Combust. Flame* **2022**, *237*, 111863. [[CrossRef](#)]
35. Cai, L.; Jacobs, S.; Langer, R.; vom Lehn, F.; Heufer, K.A.; Pitsch, H. Auto-ignition of oxymethylene ethers (OMEn, n = 2–4) as promising synthetic e-fuels from renewable electricity: Shock tube experiments and automatic mechanism generation. *Fuel* **2020**, *264*, 116711. [[CrossRef](#)]
36. He, T.; Wang, Z.; You, X.; Liu, H.; Wang, Y.; Li, X.; He, X. A chemical kinetic mechanism for the low- and intermediate-temperature combustion of Polyoxymethylene Dimethyl Ether 3 (PODE3). *Fuel* **2018**, *212*, 223–235. [[CrossRef](#)]
37. Goodwin, D.G.; Moffat, H.K.; Speth, R.L. Cantera: An object-oriented software toolkit for chemical kinetics, thermodynamics, and transport processes. *Zenodo* **2022**. [[CrossRef](#)]
38. Zhu, Q.; Zong, Y.; Tan, Y.R.; Lyu, J.-Y.; Pan, J.; Zhou, X.; Liu, H.; He, S.; Chen, W.; Yu, W.; et al. Comparative analysis of PODE3 and PODE4 fuel additives for emission reduction and soot characteristics in compression ignition engines. *Energy* **2024**, *286*, 129498. [[CrossRef](#)]
39. Niu, B.; Jia, M.; Chang, Y.; Duan, H.; Dong, X.; Wang, P. Construction of reduced oxidation mechanisms of polyoxymethylene dimethyl ethers (PODE1–6) with consistent structure using decoupling methodology and reaction rate rule. *Combust. Flame* **2021**, *232*, 111534. [[CrossRef](#)]
40. Burke, U.; Metcalfe, W.K.; Burke, S.M.; Heufer, K.A.; Dagaut, P.; Curran, H.J. A detailed chemical kinetic modeling, ignition delay time and jet-stirred reactor study of methanol oxidation. *Combust. Flame* **2016**, *165*, 125–136. [[CrossRef](#)]
41. Otomo, J.; Koshi, M.; Mitsumori, T.; Iwasaki, H.; Yamada, K. Chemical kinetic modeling of ammonia oxidation with improved reaction mechanism for ammonia/air and ammonia/hydrogen/air combustion. *Int. J. Hydrogen Energy* **2018**, *43*, 3004–3014. [[CrossRef](#)]
42. Glarborg, P.; Miller, J.A.; Ruscic, B.; Klippenstein, S.J. Modeling nitrogen chemistry in combustion. *Prog. Energy Combust. Sci.* **2018**, *67*, 31–68. [[CrossRef](#)]
43. Snegirev, A. Perfectly stirred reactor model to evaluate extinction of diffusion flame. *Combust. Flame* **2015**, *162*, 3622–3631. [[CrossRef](#)]
44. Yu, C.; Cai, L.; Chen, J.-Y. Stochastic Modeling of Partially Stirred Reactor (PaSR) for the Investigation of the Turbulence-Chemistry Interaction for the Ammonia-Air Combustion. *Flow Turbul. Combust.* **2023**, *112*, 509–536. [[CrossRef](#)]

Disclaimer/Publisher’s Note: The statements, opinions and data contained in all publications are solely those of the individual author(s) and contributor(s) and not of MDPI and/or the editor(s). MDPI and/or the editor(s) disclaim responsibility for any injury to people or property resulting from any ideas, methods, instructions or products referred to in the content.